The Journal of Chemical Physics

New insights into the early stage nucleation of calcium carbonate gels by reactive molecular dynamics simulations

Cite as: J. Chem. Phys. **157**, 234501 (2022); https://doi.org/10.1063/5.0127240
Submitted: 20 September 2022 • Accepted: 28 November 2022 • Accepted Manuscript Online: 28 November 2022 • Published Online: 15 December 2022

Ling Qin, Xingtai Mao, Yifei Cui, et al.

The Journal of Chemical Physics ARTICLE scitation.org/journal/jcp

New insights into the early stage nucleation of calcium carbonate gels by reactive molecular dynamics simulations

Cite as: J. Chem. Phys. 157, 234501 (2022); doi: 10.1063/5.0127240
Submitted: 20 September 2022 • Accepted: 28 November 2022 •
Published Online: 15 December 2022

View Online Export Citation CrossMark

Ling Qin,[1,2,3] Xingtai Mao,[1] Yifei Cui,[1,2] Jiuwen Bao,[1,2] Gaurav Sant,[4] Tiefeng Chen,[5] Peng Zhang,[1,2,a)] Xiaojian Gao,[5,6,a)] and Mathieu Bauchy[3,4,a)]

AFFILIATIONS

[1] School of Civil Engineering, Qingdao University of Technology, Qingdao 266033, China
[2] Engineering Research Center of Concrete Technology under Marine Environment, Ministry of Education, Qingdao 266520, China
[3] Physics of AmoRphous and Inorganic Solids Laboratory (PARISlab), Department of Civil and Environmental Engineering, University of California, Los Angeles, California 90095, USA
[4] Institute for Carbon Management (ICM), University of California, Los Angeles, California 90095, USA
[5] School of Civil Engineering, Harbin Institute of Technology, Harbin 150090, China
[6] Key Lab of Structures Dynamic Behavior and Control of the Ministry of Education, Harbin Institute of Technology, Harbin 150090, China

[a)] **Authors to whom correspondence should be addressed:** peng.zhang@qut.edu.cn; gaoxj@hit.edu.cn; and bauchy@ucla.edu

ABSTRACT

The precipitation of calcium carbonate ($CaCO_3$) is a key mechanism in carbon capture applications relying on mineralization. In that regard, Ca-rich cementitious binders offer a unique opportunity to act as a large-scale carbon sink by immobilizing CO_2 as calcium carbonate by mineralization. However, the atomistic mechanism of calcium carbonate formation is still not fully understood. Here, we study the atomic scale nucleation mechanism of an early stage amorphous $CaCO_3$ gel based on reactive molecular dynamics (MD) simulations. We observe that reactive MD offers a notably improved description of this reaction as compared to classical MD, which allows us to reveal new insights into the structure of amorphous calcium carbonate gels and formation kinetics thereof.

I. INTRODUCTION

Concrete is the most widely manufactured material in the world. Concrete's worldwide production is expected to rise from today's 7.3 × 10^9 cubic meters to 9.7 × 10^9 cubic meters by 2050.[1] As the world's population increases, the demand for building construction and other infrastructures is likely to continue growing, thus leading to a continuous increase in concrete's use. As a cementitious material, cement is the essential component of concrete as the cement paste forming upon cement hydration constitutes the binding phase of concrete and is responsible for its strength.[2] Cement, which represents around 10% of the total concrete mass, saw an annual production of 4.6 Gt in 2015, which is estimated to rise to 6.0–13.5 Gt/a by 2050.[1] This growth is mostly driven by China, which comprises 60% of the total worldwide production. Cement alone accounts for at least 70% of greenhouse gas emissions related to concrete production[3,4] and, altogether, for about 9% of total anthropogenic CO_2 emissions.[5–7] Therefore, it is imperative to reduce the carbon footprint of the cement concrete industry, and many efforts have been made to achieve the lower-carbon of cement.[8–10]

As an alternative, complementary route to decreasing its carbon footprint, concrete can also be used as a carbon sink by immobilizing CO_2.[11] Indeed, as a Ca-containing material, the cementitious phases in concrete can capture and sequestrate CO_2 by forming calcium carbonate ($CaCO_3$).[12] There are three main ways to achieve this goal, which includes: (i) direct carbonation of concrete raw materials, including recycled aggregates, waste cement, or

other cementitious materials before the mixing of concrete,[11,13–15] (ii) injecting CO_2 to fresh concrete during the mixing period,[16–18] and (iii) carbonation curing of the concrete.[19–21] It is worth pointing out that carbonation can be beneficial and create value—for instance, the carbonation of recycled aggregates can increase their density and minimize their porosity, which, in turn, can enhance their mechanical performance.[13–15] The carbonation of fresh concrete and carbonation curing can also improve the cement performance in concrete, but the associated carbon uptake is typically limited.[12] In contrast, the carbonation curing approach can typically result in about 3 to 4 times more carbon uptake.[22] Therefore, carbonation curing has been the most used method and is attracting more and more researchers' attention.

Upon carbonation curing, Ca cations react with dissolved carbonate species in solution to form calcium carbonate ($CaCO_3$).[23] Since the formed $CaCO_3$ typically shows a larger molar volume than non-carbonated phases, it tends to fill the pores in concrete, thereby improving the mechanical performance and durability of concrete.[24,25] The carbonation reaction usually occurs via the dissolution–precipitation process. During this process, solid Ca-rich phases, such as portlandite, $Ca(OH)_2$, dissolve in the aqueous situation and react with the dissolved carbonate species to form an amorphous hydrated precursor $CaCO_3$ gels. Finally, a crystalline calcium carbonate phase forms after the drying and crystallization of the amorphous precursors.[26–28] Therefore, understanding the formation mechanism of amorphous $CaCO_3$ gels is critical since the amorphous $CaCO_3$ gel usually serves as a metastable precursor before the crystalline $CaCO_3$ formation. Nevertheless, most of the previous studies have focused on the macroscale properties of carbonated cement and less research has been carried out on the atomic-scale mechanism of carbonation in cement pastes.[27,29,30] In other words, the atomic scale nucleation mechanism of $CaCO_3$ in aqueous conditions relevant to cementitious environments is still largely unknown. Understanding the atomic-scale mechanism of carbonation could accelerate the development of new carbonated cement binders with enhanced properties or carbon uptake by establishing a sound scientific foundation behind a process that has remained largely empirical thus far.

In that regard, molecular dynamics (MD) simulations can provide valuable insights into atomic-scale gel precipitation mechanisms and offer an alternative approach to experiments.[31,32] Indeed, during the early nucleation process, MD simulations can directly yield as an output the time-dependent atomic structure, which is typically "invisible" to experiments due to the small volume of the phases and the fast timescale.[33] In particular, MD provides a convenient way to simulate chemical reactions in large systems thanks to the recent development of reactive forcefields (e.g., ReaxFF).[34] Importantly, properly parameterized reactive forcefields can yield an accuracy that matches that offered by *ab initio* simulations while retaining a computational cost that is comparable to that of classical forcefields.[34–36] In detail, reactive forcefields can account for dynamic charge transfers between atom charges, describe the formation or breakage of bonds, and adjust the interatomic forcefield according to each atom's local environment.[36] These features make reactive forcefields an ideal approach to model systems featuring some level of chemical reactivity and disorder. Such forcefields have, for instance, been widely used to study the reactivity of silicate phases in aqueous environments.[31,33] However, the carbonation reaction in cementitious materials is yet to be modeled by reactive forcefields and, hence, this problem has not thus far benefited from the advances offered by this emerging class of forcefields.

Here, in order to reveal the atomic scale formation mechanism of $CaCO_3$ in carbonation curing of cementitious materials, we use reactive MD to investigate the early stage nucleation of $CaCO_3$. We simulate the evolution of the gel structure and network connectivity during gelation and of the kinetics thereof. We compare the predictions of a reactive forcefield (ReaxFF) with those of a conventional classical forcefield. These predictions are compared, discussed, and validated based on experimental data, when available. Our results reveal that ReaxFF offers an improved description of the gelation of carbon carbonate as compared to that offered by a classical forcefield, which, in turn, allows us to reveal new insights into the time-dependent structure of $CaCO_3$ gels.

II. METHODS

A. Simulated methodology

We conduct our simulations by using the large-scale atomic/molecular massively parallel simulation (LAMMPS) package.[37] To model the gelation of a $CaCO_3$ gel in cementitious conditions, we simulate an aqueous solution comprising dissolved Ca^{2+} cations (arising from the dissolution of Ca-rich cementitious materials) and CO_3^{2-} species (resulting from the dissolution and reaction of CO_2). The simulation system comprises 3150 atoms with a $Ca^{2+}/CO_3^{2-}/H_2O$ molar ratio of 30/30/1000, that is, the Ca^{2+} concentration is 1.67×10^{-3} mol/l. For comparison, the solubility of $Ca(OH)_2$ in cement pore solutions is about 22×10^{-3} mol/l.[38] The Ca^{2+} concentration adopted in our simulation is based on previous experiments on calcium carbonate mineral formation (in which the adopted Ca^{2+} concentration ranges from 0.2×10^{-3} to 2×10^{-3} mol/l)[39] and simulation results (Ca^{2+}/H_2O = 30/1000) as described in Ref. 40. In order to maintain the neutrality of the simulation system, the concentration of CO_3^{2-} is kept equal to that of Ca^{2+}.[40] First, we use the PACKMOL package to randomly place isolated Ca^{2+}, CO_3^{2-} species, and H_2O molecules in a cubic simulation box with a length size of 40 Å featuring periodic boundary conditions.[41] A cutoff of 4 Å is used in between the species to avoid any unrealistic overlap between atoms. Ow and Oc represent the O atoms that belong to H_2O and CO_3^{2-}, respectively. Ot is the total number of O atoms in the simulation system, that is, Ot = Ow + Oc. A snapshot of the initial configuration of the simulated amorphous calcium carbonate system is presented in Fig. 1. The simulation system is then relaxed for 20 ns in an isothermal–isobaric (*NPT*) ensemble under 1 atm of pressure and various temperatures (namely, 300, 325, 350, 400, and 450 K) by using the barostat and Nosé–Hoover thermostat as described in Refs. 42 and 43. The densities of the simulation system obtained after 20 ns NPT equilibration are about 1.001, 0.979, 0.951, 0.910, and 0.821 g/cm^3, respectively, when the simulation temperatures are 300, 325, 350, 400, and 450 K, which are in accordance with those of aqueous solution. In order to describe the motion of the atoms, we use the velocity-Verlet integration algorithm with a time step of 0.25 fs.

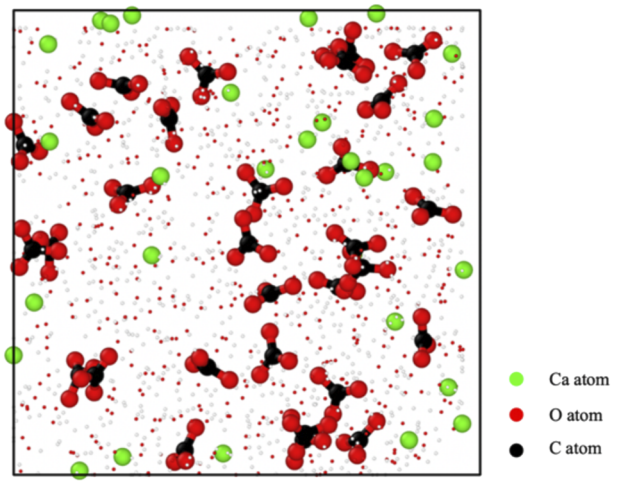

FIG. 1. Initial configuration of the simulated amorphous calcium carbonate system. Ca, C, O, and H atoms are colors in green, black, red, and white, respectively. H_2O molecules are represented as smaller atoms for clarity.

B. Simulation forcefields

Two types of forcefields (classical and reactive) are selected and compared. First, we consider the classical forcefield, which was parameterized by Raiteri *et al.*[44] This forcefield models the atoms as rigid ions, and the charges of the atoms are fixed.[44] This forcefield has been shown to provide a realistic description of carbonate solutions.[44] Second, we use the reactive ReaxFF forcefield, which was parameterized by Gale *et al.*[45] Recently, a new ReaxFF forcefield related to metallic carbonate systems (including CO_3^{2-} anion and Ca^{2+}, Na^+, and Mg^{2+} cations) has been developed by Dasgupta *et al.*,[46] which is fully transferable with previous ReaxFF water and water/electrolyte descriptions. It will be investigated and utilized in the subsequent work. ReaxFF is a forcefield based on a bond order formulation, and it can describe chemical bonds' breakdown or formation dynamics by calculating the interatomic bond order. The interatomic bond order is dependent on each atom's local environment. The total energy of the ReaxFF system (E_{sys}) can be described by ten energy terms, as shown in the following equation:[34,45–47]

$$E_{sys} = E_{bond} + E_{Coulomb} + E_{VdWaals} + E_{under} + E_{lp} + E_{over} + E_{tors} + E_{val} + E_{pen} + E_{conj}, \quad (1)$$

where E_{bond} is the short-range bond energy, $E_{Coulomb}$ the Coulomb potential energy, $E_{VdWaals}$ the van der Waals energy, E_{under} the under-coordination energy, E_{lp} the long-range electron pair energy, E_{over} the over-coordination energy, E_{tors} the torsion energy, E_{val} the valence angle energy, E_{pen} the penalty energy, and E_{conj} the conjugation energy. Among these ten energy terms, the covalent terms (including short-range bond energy, torsion energy, and valence angle energy) originate from the general relationship between the interatomic distances and dynamic bond order. A more detailed description of these ten energy terms can be referred to in Refs. 34 and 47. Moreover, unlike the classical forcefield, which relies on fixed charges, ReaxFF dynamically determines the atom charge according to the charge equilibration approach[48,49] based on the electron affinities and atomic radii, etc. As such, according to each atom's local environment and model chemical reactions, ReaxFF can adjust the energy terms. These abilities enable ReaxFF to simulate defected and disordered materials and the reactivity thereof.[50,51] It should be noted that the classical forcefield is significantly faster than ReaxFF. Specifically, in order to achieve a simulation time of 20 ns, the simulation time [in central processing unit (CPU) hours] for the reactive forcefield and classical forcefield is 2760 and 54 h, respectively, when the simulation temperature is 300 K.

C. Structural analysis

In order to describe the atomic structure and topology of amorphous $CaCO_3$ gels, we calculate each atom's partial coordination number by counting the number of neighboring atoms in its first coordination shell. Here, for each atomic pair, the radial extent of the first coordination shell is defined as the minimum distance after the first peak in the partial pair distribution functions (PDFs), which yield a cutoff value of 2.3 and 3.2 Å for C–O and Ca–O bonds, respectively. C–O and Ca–O bonds (and Ca–O–C linkages) in amorphous calcium carbonate gel structures can then be identified according to these atomic pair cutoffs. Next, we track the time-dependent evolution of the network connectivity during gelation and the kinetics thereof. The visualization of the simulated structure is realized by the Ovito software.[52]

III. RESULTS AND DISCUSSION

A. Evolution of the network connectivity during gelation

To reveal the evolution of the network connectivity upon gelation, we first investigate the connectivity of the Ca atoms as a function of time when the temperature is 300 K. The evolution of the number of Ca–O bonds per Ca atom (that is, the Ca–O partial coordination number) as a function of time is shown in Fig. 2. Overall, we find that the total coordination number of Ca atoms (Ca–Ot/Ca molar ratio) remains fairly stable throughout the gelation process—at around 6.8 and 7.5 for the reactive and classical forcefields, respectively. Nevertheless, we find that the type of the O atoms that are present in the first coordination shell of the Ca atoms notably changes as a function of time for both the classical and reactive forcefields. As expected, initially, the Ca atoms are completely surrounded by Ow atoms, which means the Ca^{2+} ions initially act as isolated hydrated cations. Upon increasing simulation time, the Ca–Oc bonds gradually replace the Ca–Ow bonds. This indicates that the Ca atoms begin to form bonds with O atoms belonging to CO_3^{2-} species. The formation of Ca–Oc–C linkages leads to the appearance of carbonate clusters. Figure 3 shows some snapshots of the amorphous $CaCO_3$ system after various gelation times. According to Fig. 3, it can also be clearly observed that Ca^{2+} ions are initially isolated in the early configuration [Fig. 3(a)], but, as time increases, CO_3^{2-} species start to interconnect via Ca atoms by forming C–Oc–Ca–Oc–C linkages. Overall, the degree of polymerization of $CaCO_3$ gels gradually increases over time for both the classical and reactive forcefields [Figs. 3(b1) and 3(c2)]. However, the two forcefields predict notably

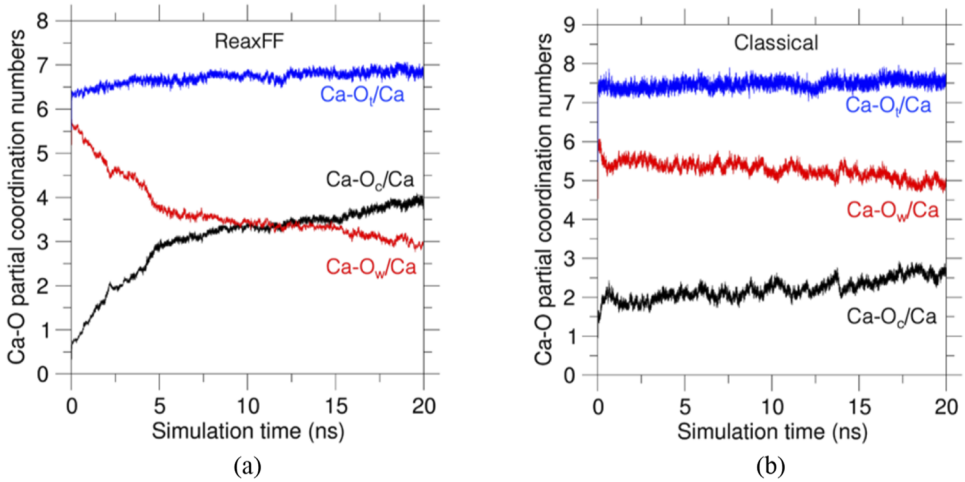

FIG. 2. Evolution of the Ca–O partial coordination numbers as a function of the gelation time at 300 K, as predicted by the (a) reactive and (b) classical forcefields.

different rates of bond formation and final value thereof. Specifically, we find that the replacement of Ca–Ow by Ca–Oc predicted by the ReaxFF forcefield occurs faster than that shown by the classical forcefield (Fig. 2). In addition, we note that the final number of Ca–Oc bonds per Ca predicted by ReaxFF (4.3) is higher than that predicted by the classical forcefield (2.5). This indicates that ReaxFF predicts a more polymerized calcium carbonate gel that yielded by the classical forcefield. This phenomenon can also be observed in Figs. 3(c1) and 3(c2).

Figure 4 exhibits the time evolution of the number of Ca–O–C linkages per Ca atom predicted by the two forcefields. We find that both forcefields yield a gradual increase in the number of Ca–O–C linkages over time, which confirms that the polymerization degree of calcium carbonate gels gradually increases upon gelation. We find that the final number of Ca–O–C linkages per Ca atom predicted by ReaxFF is about 1.6, which is larger than that yielded by the classical forcefield (1.2). This confirms that ReaxFF predicts a more polymerized calcium carbonate gel than the classical forcefield, in agreement with the results shown in Figs. 2 and 3.

To evaluate the diffusivity of H_2O and CO_3 molecules, we calculate the mean square displacement (MSD) values of Ow and Oc predicted by the reactive and classical forcefields (as shown in Fig. 5). We find that all MSD curves move to the diffusion stage after 60 ps, where the MSD is proportional to time (t). The diffusion constant (D) can be expressed by the following equation:

$$\mathrm{D}(t) = \mathrm{dMSD}(t)/6\mathrm{d}t \approx \mathrm{MSD}(t)/6t. \tag{2}$$

When the MSD is proportional to time, Eq. (2) can be transformed into the following equation:

$$\ln \mathrm{MSD}(t) = \ln t + \ln(6D). \tag{3}$$

According to Fig. 5, the diffusion constants of water and CO_3 predicted by the reactive and classical forcefields are 0.108 and 0.033, 0.175 and 0.076 Å^2/ps, respectively. Therefore, the diffusions of water and CO_3 predicted by the classical forcefield are faster than those predicted by the reactive forcefield. Thus, the classical forcefield converges much faster upon its final number of Ca–O–C linkages (as shown in Fig. 4).

B. Polymerization kinetics

In order to characterize the kinetics of the gelation process, we explore the influence of temperature on the polymerization process of calcium carbonate gels. Therefore, we track the time evolution of the number of Ca–Oc bonds under different reaction temperatures for both the reactive forcefield and classical forcefield (see Fig. 6). We observe that, as expected, the number of Ca–Oc bonds per Ca increases faster upon increasing temperature for both the forcefields.

To quantify the kinetics of the gelation process, we calculate the polymerization rate k of the reaction for each temperature by fitting the Ca–Oc(t) curves presented in Fig. 6 by an exponential first-order relaxation function as follows:

$$\mathrm{Ca-Oc/Ca}(t) = A[1 - \exp(-kt)], \tag{4}$$

where A is the final number of Ca–Oc bonds per Ca at infinite simulation time and t is the gelation time. Figure 7 shows the resulting polymerization rates. We find that the calcium carbonate polymerization rate increases upon increasing temperature for both the forcefields. However, we find that the polymerization rates predicted by the classical forcefield are systematically about an order of magnitude larger than those obtained with ReaxFF. According to Fig. 7, we also find that the polymerization rate displays an Arrhenius-like dependence on temperature T. Based on the Arrhenius relationship,[53] the activation energy E_A of the polymerization reaction can be calculated as

$$k(T) = k_0 \cdot \exp(-E_A/RT), \tag{5}$$

where T, k_0, and R are the temperature, polymerization rate at infinite temperature, and universal gas constant, respectively.

The obtained activation energies of the polymerization reaction are shown in Fig. 8. The polymerization activation energies predicted by the reactive forcefield and the classical forcefield are 6.63 ± 0.12 and 5.39 ± 0.14 kJ/mol, respectively. These values can

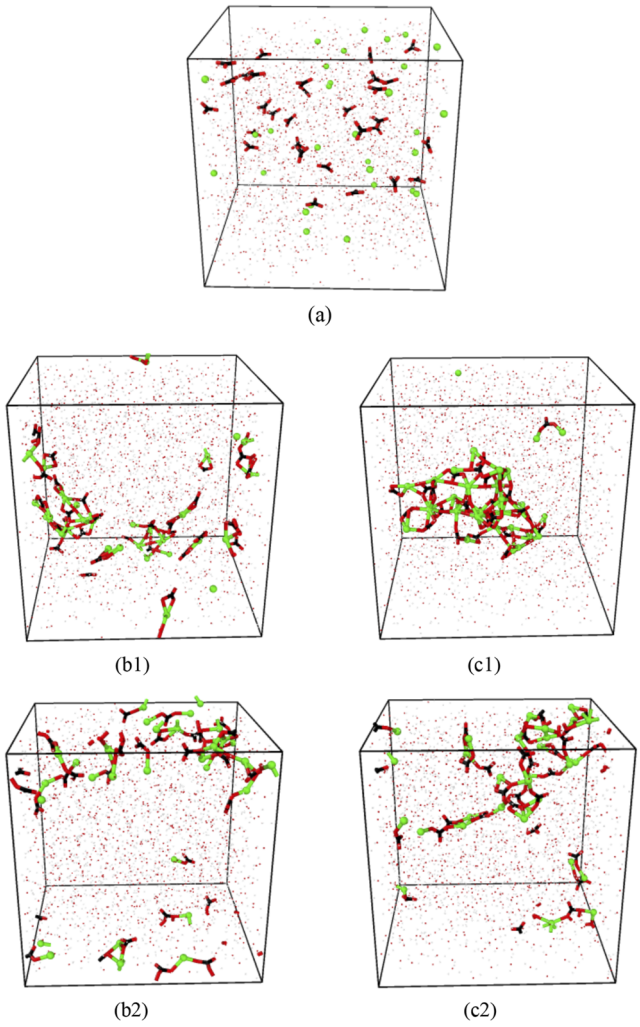

FIG. 3. Snapshots of the amorphous $CaCO_3$ system after (a) 0 ns, (b) 7 ns, and (c) 20 ns of gelation at 300 K, as predicted by the (1) reactive and (2) classical forcefields.

be compared with available experimental values, which span over 6–7 kJ/mol.[11,54] This suggests that the classical forcefield tends to underestimate the polymerization energy barrier and, thus, overestimate $CaCO_3$ gelation kinetics. In contrast, we find that ReaxFF offers an activation energy value that exhibits a better match with available experimental data. These results suggest that, on account of its more sophisticated formulation, the ReaxFF forcefield provides a more realistic description of the calcium carbonate gelation process.

C. Structure of the calcium carbonate gel

Having established that ReaxFF provides a more realistic description of the calcium carbonate gelation kinetics, we now explore the effect of the forcefield on the final atomic structure of the amorphous $CaCO_3$ gel forming at the end of the simulation (at 300 K). To investigate the short-range structure of the simulated

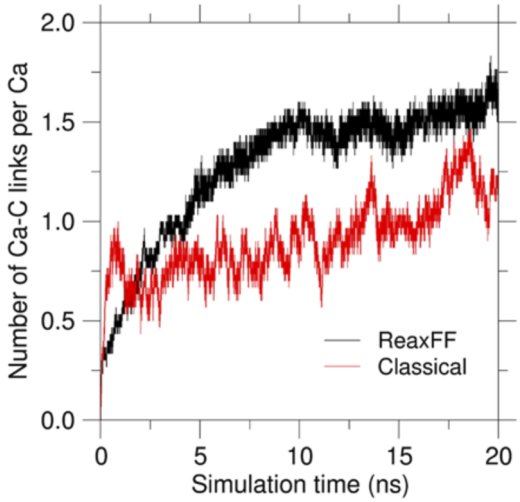

FIG. 4. Time evolution of the number of Ca–O–C linkages per Ca atom at 300 K.

gel, we calculate the average distance between Ca–O, Ca–Ca, and Ca–C interatomic pairs and the coordination number of Ca atoms predicted by the reactive and classical forcefields and, whenever available, compare the results with the experimental results sourced from Ref. 39. The distance between atomic pairs can be obtained from the PDFs presented in Fig. 9. The PDF captures the probability of finding other particles at a distance r from any specified "central" particle.[55] As expected, all the computed pair distributions converge toward 1 at a large distance, which indicates that the simulated gels do not exhibit any long-range order. However, Fig. 9 reveals the existence of some notable differences in the short-range order structure (i.e., $r < 5$ Å) predicted by the two forcefields. First, we observe that, in general, the peaks predicted by ReaxFF are notably sharper than those predicted by the classical forcefield. This indicates that ReaxFF yields a gel structure that is more locally ordered (with more well-defined interatomic distances) than the classical forcefield. We also find that the first peak in the Ca–Ca and Ca–C partial PDFs predicted by ReaxFF shifts toward lower r values as compared to what is

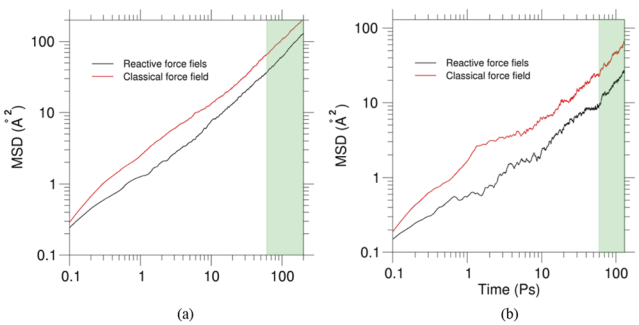

FIG. 5. Time evolution of the mean square displacement of (a) Ow and (b) Oc atoms at 300 K.

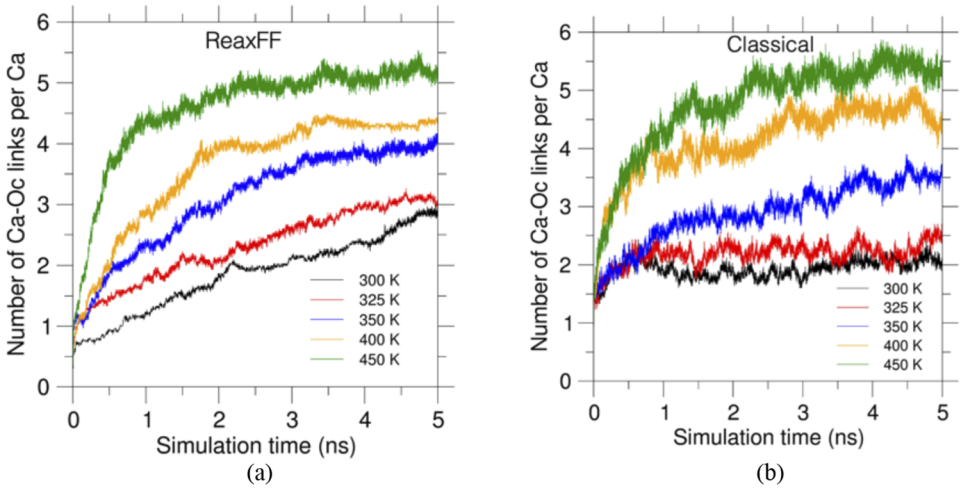

FIG. 6. Time evolution of the number of Ca–Oc bonds per Ca atom under select temperatures, as predicted by the (a) reactive and (b) classical forcefields.

yielded by the classical forcefield. This suggests that, overall, ReaxFF predicts a more compact gel structure, wherein the cations are closer to each other as compared to the structure predicted by the classical forcefield.

Next, we use the computed PDFs to determine the average Ca–O, Ca–Ca, and Ca–C interatomic distances predicted by the two forcefields and compare them with the experimental data reported in Ref. 39. Two Ca–O distances (referred to as Ca–O_1 and Ca–O_2 distances) were defined in Ref. 39, wherein Ca–O_1 and Ca–O_2 refer to the first and second coordination shells of oxygen atoms around Ca atoms, respectively.[39] The Ca–O_1 distance from Ref. 39 can be directly compared with the position of the first peak in the Ca–O PDFs shown in Fig. 9(a). The computed average Ca–Ca and Ca–C interatomic distances are calculated based on the average position of the peaks in the associated partial PDFs within the range of the first coordination shell. It should be noted that simulations and experiments were conducted at the same temperature (300 K) and at a fairly similar Ca^{2+} concentration (2×10^{-3} and 1.67×10^{-3} mol/l for the experiment and simulation, respectively), so that a direct comparison is possible. We nevertheless acknowledge that this comparison could be affected by the limited timescale of the simulation. Figure 10 shows the average interatomic distances offered by the two forcefields as well as a comparison with the experimental values. The Ca–O, Ca–Ca, and Ca–C interatomic distances predicted by the reactive and classical forcefields are 2.38, 4.21, 3.22 and 2.46, 4.91, 3.17 Å, respectively. For comparison, associated experimental data are 2.37 ± 0.04, 4.15 ± 0.04, and 3.24 ± 0.04 Å, respectively. Overall, we find that ReaxFF yields a significantly improved match

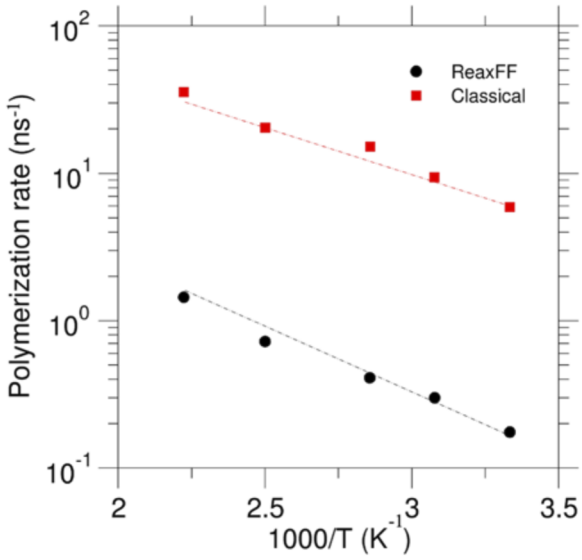

FIG. 7. Polymerization rate of the simulated calcium carbonate gels (obtained by fitting the data shown in Fig. 6) as a function of the inverse temperature.

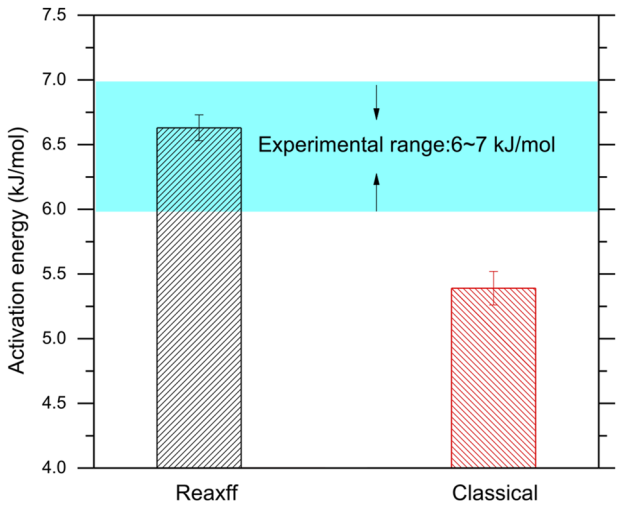

FIG. 8. Activation energy associated with the polymerization of the simulated calcium carbonate gels.

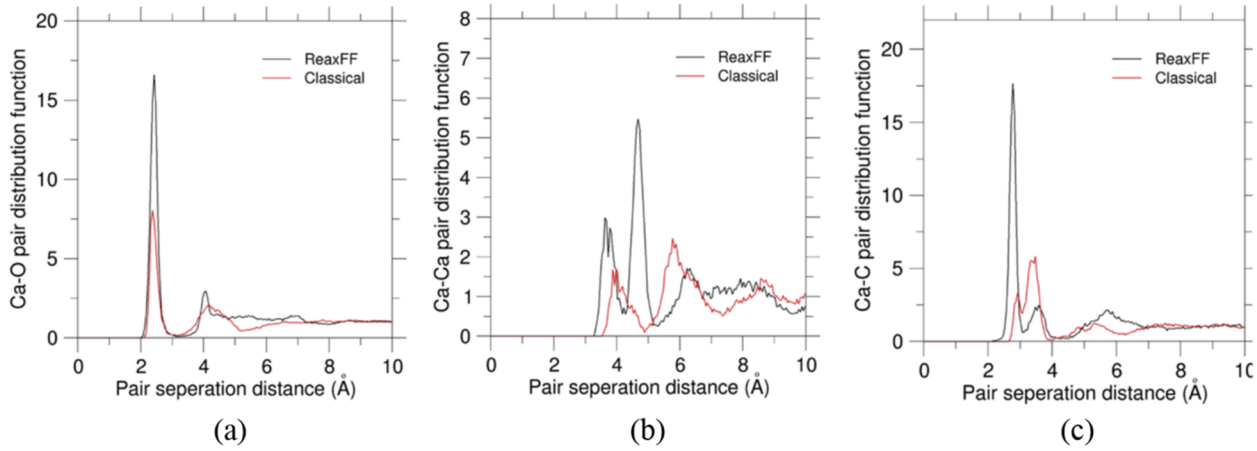

FIG. 9. (a) Ca–O, (b) Ca–Ca, and (c) Ca–C partial pair distribution functions of the amorphous calcium carbonate gels forming at the end of the simulation at 300 K.

with the experimental data (especially for the Ca–Ca interatomic distance) as compared to the classical forcefield. Specifically, the relative difference between simulation and experimental results is (for Ca–O, Ca–Ca, and Ca–C) 0.42%, 1.56%, 0.62% and 3.80%, 18.31%, 2.16%, in the case of the reactive and classical forcefields, respectively.

Finally, we compare the computed Ca–O, Ca–Ca, and Ca–C partial coordination numbers with the experimental data (see Fig. 11). The reactive and classical forcefields predict these coordination numbers to be 6.80, 1.70, 1.60 and 7.50, 1.40, 1.20, respectively. In comparison, the associated experimental data (Ca–O, Ca–Ca, and Ca–C) are 5.30, 3.25, and 1.60, respectively. Overall, we find that the simulated Ca–O and Ca–Ca coordination numbers are systematically larger and smaller than their experimental counterparts, respectively, but are consistent with previous simulation results.[27,56,57] Nevertheless, we find that ReaxFF offers a better level of agreement with the experimental data than the classical forcefield. The improvement in accuracy is especially pronounced in the case of the Ca–C partial coordination number (which captures the overall degree of polymerization of the gel).

Overall, the results presented in Figs. 8, 10, and 11 demonstrate that ReaxFF offers an overall improved description of the structure

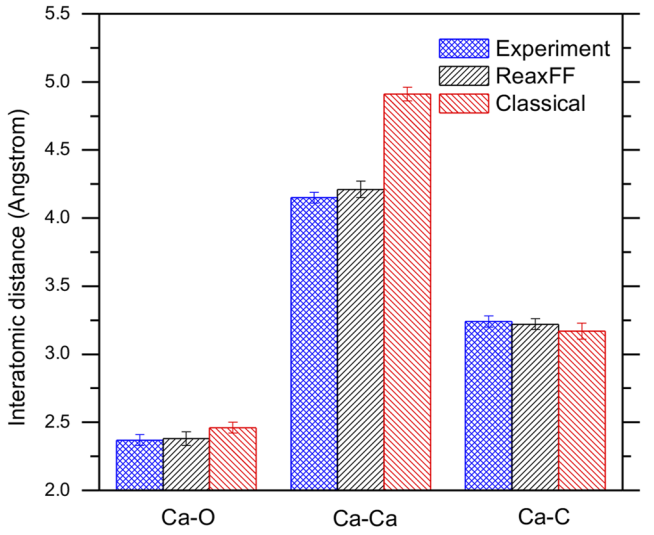

FIG. 10. Average Ca–O, Ca–Ca, and Ca–C interatomic distances in the simulated amorphous calcium carbonate gels forming at the end of the simulation at 300 K. The simulation data are compared with the experimental data sourced from Ref. 39.

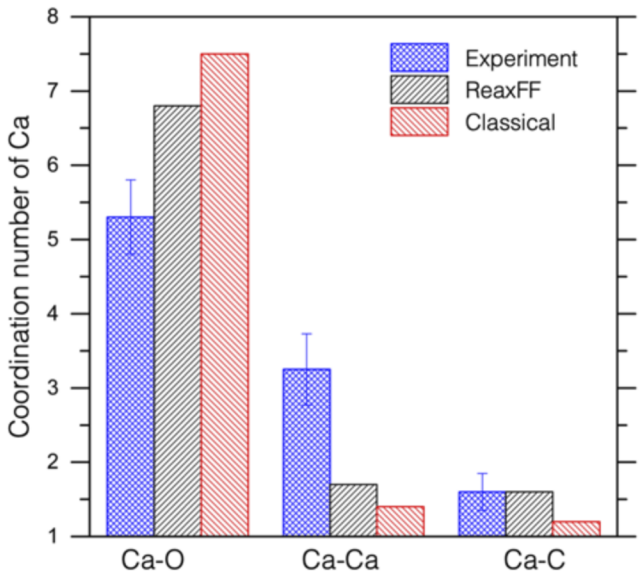

FIG. 11. Ca–O, Ca–Ca, and Ca–C partial coordination number in the simulated amorphous calcium carbonate gels forming at the end of the simulation at 300 K. The simulation data are compared with the experimental data sourced from Ref. 39.

of amorphous calcium carbonate gels as compared to MD simulations based on classical forcefields (based on a comparison with the available experimental "signatures" of the gel structure). Although this is not surprising (since the ReaxFF relies on a more complex formulation and involves a larger number of fitting parameters), this nevertheless suggests that reactive potentials offer a unique opportunity to revisit the structure and dynamics of hydrated/carbonated gels over spatial and temporal scales that are simply inaccessible to *ab initio* simulations. We envision that, going forward, machine-learned forcefields could further push these boundaries and unlock new secrets in the structure of amorphous calcium carbonate and formation mechanism thereof.

IV. CONCLUSIONS

Based on the above simulation results, we can obtain the following conclusions:

(1) Molecular dynamics offers a realistic description of the time-dependent gelation of amorphous calcium carbonate systems in aqueous conditions relevant to cementitious environments.
(2) When compared to a previous state-of-the-art classical forcefield, ReaxFF offers an increased level of agreement with available experimental data, in terms of both polymerization kinetics and final structure topology.
(3) Our reactive molecular dynamics simulations reveal that the structure of amorphous calcium carbonate gels is more polymerized and locally ordered than previously suggested by classical forcefields.

ACKNOWLEDGMENTS

This research was supported by the National Science Foundation (Grant No. DMREF-1922167), the National Natural Science Foundation of China (Grant No. 52208260), the Natural Science Foundation of Shandong province (Grant No. ZR2022QE002), and the China Scholarship Council (Grant No. 201906120295).

AUTHOR DECLARATIONS

Conflict of Interest

The authors have no conflicts to disclose.

Author Contributions

Ling Qin: Investigation (equal); Methodology (equal); Writing – original draft (equal); Writing – review & editing (equal). **Xingtai Mao**: Writing – review & editing (equal). **Yifei Cui**: Writing – review & editing (equal). **Jiuwen Bao**: Writing – review & editing (equal). **Gaurav Sant**: Writing – review & editing (equal). **Tiefeng Chen**: Writing – review & editing (equal). **Peng Zhang**: Funding acquisition (equal); Writing – review & editing (equal). **Xiaojian Gao**: Funding acquisition (equal); Writing – review & editing (equal). **Mathieu Bauchy**: Funding acquisition (equal); Supervision (equal); Writing – review & editing (equal).

DATA AVAILABILITY

The data that support the findings of this study are available from the corresponding authors upon reasonable request.

REFERENCES

[1]W. Schmidt, M. Otieno, K. Olonade, N. Radebe, H. Van-Damme, P. Tunji-Olayeni, S. Kenai, A. T. Tawiah, K. Manful, A. Akinwale, R. Mbugua, and A. Rogge, RILEM Tech. Lett. **5**, 63 (2020).
[2]G. Habert, S. A. Miller, V. M. John, J. L. Provis, A. Favier, A. Horvath, and K. L. Scrivener, Nat. Rev. Earth Environ. **1**, 559 (2020).
[3]L. Qin, X. Mao, X. Gao, P. Zhang, T. Chen, Q. Li, and Y. Cui, Case Stud. Constr. Mater. **17**, e01199 (2022).
[4]S. A. Miller, A. Horvath, and P. J. M. Monteiro, Environ. Res. Lett. **11**, 074029 (2016).
[5]S. A. Miller, V. M. John, S. A. Pacca, and A. Horvath, Cem. Concr. Res. **114**, 115 (2018).
[6]L. Qin, X. Gao, A. Su, and Q. Li, J. Cleaner Prod. **278**, 123897 (2021).
[7]L. Qin, X. Gao, and Q. Li, J. Cleaner Prod. **196**, 726 (2018).
[8]L. Wang, L. Chen, J. L. Provis, D. C. W. Tsang, and C. S. Poon, Cem. Concr. Compos. **106**, 103489 (2020).
[9]L. Proaño, A. T. Sarmiento, M. Figueredo, and M. Cobo, J. Cleaner Prod. **263**, 121457 (2020).
[10]S. Siddique, A. Naqi, and J. G. Jang, Cem. Concr. Compos. **111**, 103616 (2020).
[11]K. Vance, G. Falzone, I. Pignatelli, M. Bauchy, M. Balonis, and G. Sant, Ind. Eng. Chem. Res. **54**, 8908 (2015).
[12]Z. Liu and W. Meng, J. CO_2 Util. **44**, 101428 (2020).
[13]S. K. Kaliyavaradhan and T.-C. Ling, J. CO_2 Util. **20**, 234 (2017).
[14]V. W. Y. Tam, A. Butera, K. N. Le, and W. Li, Constr. Build. Mater. **250**, 118903 (2020).
[15]B. Zhan, C. S. Poon, Q. Liu, S. Kou, and C. Shi, Constr. Build. Mater. **67**, 3 (2014).
[16]S. Monkman and M. Macdonald, J. Cleaner Prod. **167**, 365 (2017).
[17]X. Qian, J. Wang, Y. Fang, and L. Wang, J. CO_2 Util. **25**, 31 (2018).
[18]S. Monkman, M. Macdonald, R. D. Hooton, and P. Sandberg, Cem. Concr. Compos. **74**, 218 (2016).
[19]T. Chen and X. Gao, ACS Sustainable Chem. Eng. **8**, 3872 (2020).
[20]Y. Liu, Y. Zhuge, C. W. K. Chow, A. Keegan, D. Li, P. N. Pham, J. Huang, and R. Siddique, J. Cleaner Prod. **261**, 121257 (2020).
[21]D. Zhang, T. Liu, and Y. Shao, J. Mater. Civil Eng. **32**, 04020038 (2020).
[22]T. Lim, B. R. Ellis, and S. J. Skerlos, Res. Lett. **14**, 114014 (2019).
[23]L. Qin and X. Gao, Fuel **245**, 1 (2019).
[24]L. Qin and X. Gao, Waste Manage. **89**, 254 (2019).
[25]L. Qin, X. Gao, and T. Chen, Constr. Build. Mater. **212**, 653 (2019).
[26]Y.-W. Wang, Y.-Y. Kim, C. J. Stephens, F. C. Meldrum, and H. K. Christenson, Cryst. Growth Des. **12**, 1212 (2012).
[27]Q. Zhou, T. Du, L. Guo, G. Sant, and M. Bauchy, Appl. Sci. **10**, 4359 (2020).
[28]M. G. Taylor, K. Simkiss, G. N. Greaves, M. Okazaki, and S. Mann, Proc. R. Soc. B **252**(1333), 75–80 (1993).
[29]F. M. Michel, J. MacDonald, J. Feng, B. L. Phillips, L. Ehm, C. Tarabrella, J. B. Parise, and R. J. Reeder, Chem. Mater. **20**, 4720 (2008).
[30]K. Henzler, E. O. Fetisov, M. Galib, M. D. Baer, B. A. Legg, C. Borca, J. M. Xto, S. Pin, J. L. Fulton, G. K. Schenter, N. Govind, J. I. Siepmann, C. J. Mundy, T. Huthwelker, and J. J. De Yoreo, Sci. Adv. **4**, eaao6283 (2018).
[31]T. Du, H. Li, G. Sant, and M. Bauchy, J. Chem. Phys. **148**, 234504 (2018).
[32]M. Wang, M. M. Smedskjaer, J. C. Mauro, M. Bauchy, and M. Modifier, J. Chem. Phys. **150**, 044502 (2019).
[33]T. Du, H. Li, Q. Zhou, Z. Wang, G. Sant, J. V. Ryan, and M. Bauchy, npj Mater. Degrad. **3**, 6 (2019).
[34]A. C. T. van Duin, S. Dasgupta, F. Lorant, and W. A. Goddard, J. Phys. Chem. A **105**, 9396 (2001).
[35]C. Mischler, W. Kob, and K. Binder, Comput. Phys. Commun. **147**, 222 (2002).

[36]C. Zhao, W. Zhou, Q. Zhou, Y. Zhang, H. Liu, G. Sant, X. Liu, L. Guo, and M. Bauchy, J. Chem. Phys. **153**, 014501 (2020).
[37]S. Plimpton, J. Comput. Phys. **117**, 1 (1995).
[38]A. Pallagi, Á. Tasi, A. Gácsi, M. Csáti, I. Pálinkó, G. Peintler, and P. Sipos, Cent. Eur. J. Chem. **10**, 332 (2012).
[39]J. Avaro, E. M. Moon, J. Rose, and A. L. Rose, Geochim. Cosmochim. Acta **259**, 344 (2019).
[40]P. J. M. Smeets, A. R. Finney, W. J. E. M. Habraken, F. Nudelman, H. Friedrich, J. Laven, J. J. De Yoreo, P. M. Rodger, and N. A. J. M. Sommerdijk, Proc. Natl. Acad. Sci. U. S. A. **114**(38), E7882 (2017).
[41]L. Martínez, R. Andrade, E. G. Birgin, and J. M. Martínez, J. Comput. Chem. **30**, 2157 (2009).
[42]W. Shinoda, M. Shiga, and M. Mikami, Phys. Rev. B **69**, 134103 (2004).
[43]M. E. Tuckerman, J. Alejandre, R. López-Rendón, A. L. Jochim, and G. J. Martyna, J. Phys. A: Math. Gen. **39**, 5629 (2006).
[44]P. Raiteri, R. Demichelis, and J. D. Gale, J. Phys. Chem. C **119**, 24447 (2015).
[45]J. D. Gale, P. Raiteri, and A. C. T. van Duin, Phys. Chem. Chem. Phys. **13**, 16666 (2011).
[46]N. Dasgupta, C. Chen, and A. C. T. van Duin, Phys. Chem. Chem. Phys. **24**, 3322 (2022).
[47]A. C. T. van Duin, A. Strachan, S. Stewman, Q. Zhang, X. Xu, and W. A. Goddard, J. Phys. Chem. A **107**, 3803 (2003).
[48]A. K. Rappe and W. A. Goddard III, J. Phys. Chem. **95**, 3358 (1991).
[49]E. Demiralp, T. Çağin, and W. A. Goddard III, Phys. Rev. Lett. **82**, 1708 (1999).
[50]Y. Yu, B. Wang, M. Wang, G. Sant, and M. Bauchy, J. Non-Cryst. Solids **443**, 148 (2016).
[51]Y. Yu, B. Wang, M. Wang, G. Sant, and M. Bauchy, Int. J. Appl. Glass Sci. **8**, 276 (2017).
[52]A. Stukowski, Modell. Simul. Mater. Sci. Eng. **18**, 015012 (2010).
[53]S. G. E. Giap, J. Phys. Sci. **21**(1), 29–39 (2010).
[54]G. Montes-Hernandez, R. Chiriac, and F. Toche, Int. J. Greenhouse Gas Control **11**(1), 172–180 (2012).
[55]T. Proffen, S. J. L. Billinge, T. Egami, and D. Louca, Z. Kristallogr. - Cryst. Mater. **218**, 132 (2003).
[56]L. X. Dang, G. K. Schenter, and J. L. Fulton, J. Phys. Chem. B **107**, 14119 (2003).
[57]D. Di Tommaso, E. Ruiz-Agudo, N. H. de Leeuw, A. Putnis, and C. V. Putnis, Phys. Chem. Chem. Phys. **16**, 7772 (2014).